Murdoch
UNIVERSITY

MURDOCH RESEARCH REPOSITORY

This is the author's final version of the work, as accepted for publication following peer review but without the publisher's layout or pagination. The definitive version is available at
http://dx.doi.org/10.1016/j.ultsonch.2010.11.007

Brundavanam, R.K., Jiang, Z-T, Chapman, P., Le, X., Mondinos, N., Fawcett, D. and Poinern, G.E.J. (2011) ***Effect of dilute gelatine on the ultrasonic thermally assisted synthesis of nano hydroxyapatite.*** **Ultrasonics Sonochemistry, 18 (3). pp. 697-703.**

http://researchrepository.murdoch.edu.au/4090/

Copyright: © 2010 Elsevier B.V.

It is posted here for your personal use. No further distribution is permitted.

Accepted Manuscript

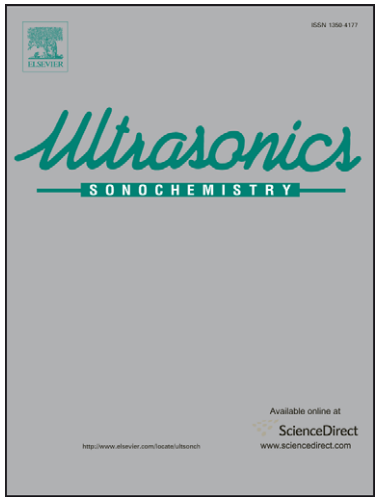

Effect of Dilute Gelatine on the Ultrasonic Thermally Assisted Synthesis of Nano Hydroxyapatite

Ravi Krishna Brundavanam, Zhong-Tao Jiang, Peter Chapman, Xuan-Thi Le, Nicholas Mondinos, Derek Fawcett, Gérrard Eddy Jai Poinern

PII: S1350-4177(10)00222-1
DOI: 10.1016/j.ultsonch.2010.11.007
Reference: ULTSON 1835

To appear in: *Ultrasonics Sonochemistry*

Received Date: 6 July 2010
Revised Date: 14 September 2010
Accepted Date: 9 November 2010

Please cite this article as: R.K. Brundavanam, Z-T. Jiang, P. Chapman, X-T. Le, N. Mondinos, D. Fawcett, r.E.J. Poinern, Effect of Dilute Gelatine on the Ultrasonic Thermally Assisted Synthesis of Nano Hydroxyapatite, *Ultrasonics Sonochemistry* (2010), doi: 10.1016/j.ultsonch.2010.11.007

This is a PDF file of an unedited manuscript that has been accepted for publication. As a service to our customers we are providing this early version of the manuscript. The manuscript will undergo copyediting, typesetting, and review of the resulting proof before it is published in its final form. Please note that during the production process errors may be discovered which could affect the content, and all legal disclaimers that apply to the journal pertain.

ACCEPTED MANUSCRIPT

Effect of Dilute Gelatine on the Ultrasonic Thermally Assisted Synthesis of Nano Hydroxyapatite

Ravi Krishna Brundavanam [a], Zhong-Tao Jiang [a], Peter Chapman [b], Xuan-Thi Le [a], Nicholas Mondinos [a], Derek Fawcett [a] and Gérrard Eddy Jai Poinern* [a]

[a] *Murdoch Applied Nanotechnology Research Group, School of Engineering and Energy, Murdoch University, Murdoch, Western Australia 6150.*

[b] *West Australian Nanochemistry Research Institute, Applied Chemistry, Curtin University, Bentley, Western Australia 6102.*

Abstract

A series of nano hydroxyapatite-gelatin composites with different dilute solutions of gelatin concentrations were synthesized by a thermally assisted low power ultrasonic irradiation method. The gelatine hydroxyapatite, (Gel-HAP) nanoparticles were prepared using $Ca(NO_3)_2$ and KH_2PO_4 in the presence of gelatine in an aqueous solution. The synthesised products were heat treated between 100°C and 400°C. The effect of the addition of gelatin on the nucleation and growth of synthesised nano HAP was investigated. Characterisation was performed using X-ray diffraction (XRD), field emission scanning electron microscopy (FE-SEM) and Fourier transform infrared spectroscopy (FT-IR). The characterisation results indicate that gelatin has been appended to the nano HAP forming regular spherical shaped crystals of nano sized Gel-HAP.

Keywords: Nano hydroxyapatite, Ultrasound irradiation, Gelatin, Chemical synthesis, Bone tissue engineering.

* Corresponding author. Tel.: +61 8 9360 2892; Fax: +61 8 9360 6183

E-mail address: g.poinern@murdoch.edu.au

ACCEPTED MANUSCRIPT

ACCEPTED MANUSCRIPT

1.0 Introduction

Bone or osseous material is a hard connective tissue that forms part of the skeletal system and is comprised of a matrix hardened by deposited calcium phosphate and other minerals. A bone disorder such as osteoporosis is a growing concern in many aging population and is associated with bone loss and development of bone brittleness and fractures. In the treatment of bone diseases, such as bone tumours and all similar defects, bone substitutes are needed in the repair/replacement of the infected bone tissue and for the treatment of fractures [1]. The preferred type of treatment involves the use of autologous bone as it displays excellent biocompatibility and osteogenic capacity but problems such as donor site morbidity and its limited supply have led to a search for artificial bone grafting materials [2]. Xenogenic and allogenic bone grafts have shown higher response from the immune system and the possibilities of pathogen transmission have led to the research and development of synthetic biocompatible materials [3]. A range of inorganic material such as calcium phosphate cements, porous coralline, and calcium sulphate material have been investigated in the past and shown to display good bioactivity [4, 5].

Calcium phosphate apatite is an important class of biomaterial with hydroxyapatite (HAP) being by far the most important biomineral, accounting for up to about 65 wt% of cortical bone and 97 wt% of dental enamel in mammalian hard tissue [6]. Natural bone is a complex living natural organic and inorganic composite material consisting of type I collagen fibrils with embedded well-arrayed nano crystalline inorganic material of HAP [7-9]. Synthetic HAP has the stoichiometric chemical formula of $Ca_{10}(PO_4)_6(OH)_2$ and HAP has been shown to exhibit excellent bone substitute qualities for hard tissues because of its biocompatibility and biodegradability. In addition, HAP has shown great stability under various physiological conditions [10-11].

ACCEPTED MANUSCRIPT

Research into nanostructures and nano synthetic methods have discovered different nano forms of HAP with many properties such as different shapes, rods, tubes, plates and spheres [12-14]. Whilst Jun *et al* showed that HAP nanoparticles inhibit the growth of hepatic tumour cells and have stronger anti-tumour effect, Li *et al* demonstrated a beneficial effect of a nanocomposite of HAP and chitosan on human gastric cancer cells [15-16]. Another advantage of HAP is that it is biocompatible as implants and provides a biological scaffold for bone formation. However, a disadvantage of pure synthetic HAP is its low load bearing capacity, which can be alleviated somehow by the addition of another material such as polylactide (PLA) and collagen whereby the mechanical properties of the HAP composite biomaterials can be significantly improved [17-19]. Many organic and inorganic based composites, such as collagen-HAP, gelatin-HAP (Gel-HAP), Polylactide-HAP composites have been prepared and reported to have significant advantages over pure HAP [20-22]. The purpose of making such composites is to improve the bone bonding and mechanical properties of HAP composite [23].

In tissue engineering there is a high demand for synthetic bone substitutes due to various diseases, accidents and age related problems. The current research interest on bone composites has focused on the fabrication of artificial bone-like nano composites such as Gel-HAP [24-25] for bone replacement therapies. Natural bone being a nano composite of HAP ceramic and organic structures such as collagen structures containing gelatine (GEL) has been a favoured option. A composite of nano size Gel-HAP can be prepared by dispersing nano HAP powders in concentrated gelatine solutions [26-28]. This method of producing nano Gel-HAP composites has the disadvantage of the nano HAP powder agglomerating, making it difficult to form a controlled structure [23]. Another method used to synthesise Gel-HAP nano composites is *via* precipitation of HAP within a gelatin gel [24, 29-31]. Using this method it is easier to develop a controlled porous structure of composites that when implanted into

ACCEPTED MANUSCRIPT

damaged bone, induces better blood circulation and bone in-growth. Kim *et al.,* developed Gel-HAP porous nanocomposites by the precipitation of HAP nano crystals within a gelatin matrix and studied their osteoblastic cellular responses in comparison to traditionally prepared Gel-HAP composites [28]. Their findings suggested that Gel-HAP nanocomposites obtained by the precipitation method showed higher degree of osteoblast cells attachment than to the conventionally made Gel-HAP micron size composites.

In the area of sonochemical synthesis of HAP, Jevtic *et al* used of unique properties of sonocrystallisation to manufacture nanorods of HAP with a high-intensity (750W system) ultrasound system [34]. In addition, a recent study by Ethirajan *et al* in 2008 has shown the value of using high-powered ultrasounds in combination with a high concentrated solution of gelatine to generate GEL-HAP nanospheres by a reverse micellar method [35]. In 2009, Poinern *et al* [36] investigations into nano HAP indicated that the size, crystal structure and morphology of pure Nano-HAP spheroids were enhanced by the use of low power ultrasonic irradiation in the synthesis process.

The present work investigates the combined effect of dilute gelatin concentration and low power ultrasound irradiation on the formation of nano HAP. A precipitation method assisted with low powered ultrasonic irradiation was used, this was then followed by a thermal treatment over a temperature range of 100 °C – 400 °C. We study the effects of low power ultrasonic irradiation on the size, morphology and crystal structure of the resulting Gel-HAP matrix. Furthermore a comparison is made with respect to the Gel-HAP matrix prepared without ultrasonic assisted synthesis. The nano Gel-HAP powders formed were characterised using X-ray diffraction (XRD), field emission scanning electron microscopy (FE-SEM) and Fourier transform infrared spectroscopy (FT-IR).

ACCEPTED MANUSCRIPT

2.0 Materials and Methods

2.1 Materials

$Ca(NO_3)_2.4H_2O$ (99% pure), KH_2PO_4 (99% pure) and ammonia solution were used as Ca^{2+}, PO_4^{3-}, and OH^- sources. All the source materials and gelatin were supplied by CHEM-SUPPLY. The ultrasonic processor was an UP50H (50 W, 30 kHz, MS7 Sonotrode (7mm diameter, 80 mm length)) by Hielscher Ultrasound Technology. MilliQ water was used throughout the experiments.

2.2 Experimental Procedure

2.5 ml of ammonia was added to 40 ml of 0.32 M $Ca(NO_3)_2{\cdot}4H_2O$ solution. The pH value of the solution at this stage was between 9 and 11. Gelatine (1 g) was completely dissolved in 1000 ml MilliQ water at 40 °C. 2 ml of the prepared gelatin solution was then added to the above Ca^{2+}/NH_3 mixture. The mixture was sonicated with 30 kHz ultrasonic irradiation source rated at a power of 50 W. At the same time 60 ml of 0.19 M KH_2PO_4 was slowly added drop wise to the above mixture. The whole solution was kept under ultrasonic irradiation for 1 hour. The pH value was checked and maintained at pH 9 at all times and the Ca/P ratio was adjusted to 1.67. The resultant white precipitate was filtered by centrifugation, which produced thick slurry. The slurry was partitioned into 4 parts. Each part was heat treated in a tube furnace for 2 hours at a specific temperature of 100 ºC, 200 ºC, 300 ºC and 400 ºC. This produced Gel-HAP powders in granular form.

The above procedure was repeated by varying the volume of stock gelatin solution concentrations set at 5, 10, 20, 40 and 100 ml respectively. The final Gel-HAP products were grinded to a fine powder and characterised using XRD, FE-SEM and FT-IR techniques.

ACCEPTED MANUSCRIPT

2.3 Characterisation

XRD spectra was recorded using a Bruker D8 diffractometer with Cu K_α (λ=1.5406 Å) incident radiation (40 kV and 30 mA). The diffraction patterns were collected at room temperature over a 2θ range from 20° to 60° at 0.04° step size with acquisition time of 2.0 seconds. The crystalline size of the synthesized HAP was calculated from the XRD pattern using the Debye-Scherrer equation and from the SEM images.

FT-IR spectroscopy was performed using a Bruker Optics IFS 66 series FT-IR spectrometer. Test samples were prepared by mixing approximately 0.2 g of HAP powder together with 1 g of spectroscopic grade Potassium Bromide (KBr) and then pressing them to into a disk at a pressure of 8 kPa. Infrared spectra were recorded in the 400 to 4000 cm^{-1} region.

The structural and morphological features of HAP powders were investigated with a field Scanning Electron Microscope (SEM). All scanning electron micrographs were taken using the high resolution field emission Zeiss 1555 VP-FESEM at 3 kV with a 30 μm aperture under 1×10^{-10} Torr pressure.

3.0 Results and Discussions

Figure 1 shows the XRD patterns of Nano-HAP with gelatine (0 ml, 2 ml, 40 ml and 100 ml) thermally treated at 400 °C with and without ultrasound assisted synthesis. The XRD patterns of all samples indicate the main phase is HAP with (h k l) indices consistent with phases incorporated in the ICDD (International Centre for Diffraction Data) databases. The Miller indices of the main observed peaks are (0 0 2), (2 1 1), (1 1 2), (3 0 0), (3 1 0), (2 2 2), (2 1 3) and (0 0 4). Peaks in the 2θ range of 23.4°- 23.7°, 26.9°- 27.4° and much lower intensity peak at 40.4°- 40.9° are consistent with $CaH_2P_2O_7$ phase (JCPDS No.41-0487) and are observed in

ACCEPTED MANUSCRIPT

all the XRD spectra indicating an impurity phase in the predominately HAP material. The XRD spectra of the 100 °C and 200 °C samples show significant and even enhanced intensity peaks in the 26.9°- 27.4° 2θ range. Taking into consideration the intensity ratio of the (002) and (211) indexed HAP peaks, known data of the calcium hydrogen phosphate phases, such as $CaH_4(PO_3)_2.H_2O$ (JCPDS 46-0494) it seems a greatly reduced $CaH_2P_2O_7$ phase and possibly diammonium hydrogen phosphate, $(NH_4)_2HPO_4$ (Acta Crystallographica B28 (1972) 2065-2069) are present in the predominately Gel-HAP phase in the 100 °C, 200 °C and 300 °C (at further reduced phase amounts) treated samples.

It is interesting to note that the (300) peak is resolved more clearly as the gelatin concentration increases from 0 to 100 ml for all samples that have been prepared with ultrasound irradiation. Concurrently the peak intensities in the 26.9°- 27.4° 2θ range decrease for the 100 ml gelatin HAP samples as the temperature increases from 100 °C to 400 °C resulting in a purer phase of nano HAP product than that obtained from non-gelatin ultrasound irradiated HAP. The FT-IR spectra for the 400 °C samples verify that this is a purer phase of nano HAP with gelatine integrated to it, as is evident from the gelatine's amide, carbonyl and C-H vibration modes. These vibration modes are not observed in the ultrasound and no ultrasound synthesised pure HAP samples.

A comparison is presented in Figure 1, of the effect of ultrasonic treatment on the formation of nano Gel-HAP in the presence of dilute solutions of gelatine and at a thermal treatment T = 400 °C. Figure 1 (i) is the XRD patterns without ultrasonic treatment and Figure 1 (ii) with ultrasonic treatment. The Crystallographic software, Jade6, indentified impurity phases of calcium hydrogen phosphate hydroxide ($Ca_9HPO_4\ (PO_4)_5OH$) in the 2θ range 23.4°– 23.7°, 26.9°– 27.4° and 31°- 45° for all samples. Comparing Figure 1(i) and Figure 1 (ii) we conclude that ultrasonic irradiation during the synthesis process has resulted in a large reduction of the $Ca_9HPO_4\ (PO_4)_5OH$ phase and sharpening of the HAP peaks (especially the

ACCEPTED MANUSCRIPT

(300) peak). The XRD results indicate that ultrasound irradiation has affected the chemical interactions of the reacting species by possibly altering the rate of formation and chemical equilibrium of the calcium hydrogen phosphate hydroxide phases.

The crystalline sizes of the synthesized Gel-HAP were calculated from the observed XRD patterns using the Debye-Scherer equation [37-38]. Calculated particle sizes (in nm) for the various gelatin concentrations, ultrasonic power and temperatures are tabulated in Table 1. Nanomaterials, due to their high surface energy tends to agglomerate when mixed into a liquid. Therefore an effective means of deagglomerating and dispersing the nanoparticles is needed to overcome the bonding forces after mixing the reactants with the dilute gelatine solution. Application of ultrasounds creates cavitations effects (high speed jets) that allows effective dispersion of the nanomaterials as it is being generated in solution. The average size range of Gel-HAP particles, over the set of gelatin concentration and temperature range, is 32 nm (± 5%). This is in excellent agreement with previous synthesis of nano HAP particle using a low power ultrasound assisted method [36] only these samples have gelatine incorporated in the nano HAP phase.

Figure 2 presents the FT-IR spectra of pure HAP and Gel-HAP (2 ml, 40 ml, 100 ml Gel. Sol.) synthesised without and with ultrasonic irradiation thermally treated at 400 °C. Figure 3 is the FT-IR spectra of gelatine. Table 2 summarises the values (cm^{-1}) of the main observed absorption peaks from the FT-IR spectra of pure HAP, Gel-HAP and gelatine. It also contains the chemical species and the type of vibrational modes that produce the absorption bands.

In Figure 2, characteristic bands for the CO_3^{-2} group are in the range 825-835 cm^{-1} (ν_2) and 1450-1470 cm^{-1} (ν_3) and found in all the synthesised samples. For pure HAP samples; non ultrasonically as well as ultrasonically treated the presence of atmospheric CO_2 interacting with the HAP alkaline reactant mixture is detected. The CO_3^{-2} replaces OH^- and tends to form

ACCEPTED MANUSCRIPT

type-B HAP [39-40]. For Gel-HAP samples (non ultrasonically, ultrasonically treated) the absorption bands are in the range of 1350-1390 cm^{-1} and is to the presence of the Ca-COO^- functional group. This is due to interaction of Ca^{+2} ions with the gelatine COO^- group in the solution to form a Ca-gelatine complex. Without the use of ultrasound irradiation, this peak intensity increases with the gelatine concentration, which allows us to postulate that both the gelatine and atmospheric CO_2 contributes to this peak. However, in the presence of ultrasonic irradiation, the peak intensity decreases as the level of gelatine increases, (fig 2(ii(b-d)). This possibly suggests that the interaction of atmospheric CO_2 with HAP is reduced and thus the formation of the Ca-COO^- species is predominantly due to Gel-HAP interactions. The FTIR data suggests that these carbonated bands become less intense with increasing thermal treatment and results in purer HAP phases being produced [24].

The characteristic amino acids groups of the gelatine molecule are identified as the four major amides in the IR spectra [41-42]. The bands 3330, 2930, 1636–1661 and 1549–1558 cm^{-1} are denoted as the A, B, I and II amide bands, respectively. The amide A and B bands are associated with the stretching vibrations of the N–H group. The amide I band originates from the C=O stretching vibration coupled to the N–H bending vibration. The amide II band arises from the N–H bending vibration coupled to the C–N stretching vibration. In the thermally treated Gel-HAP samples the positions of these four amide bands are slightly shifted from those observed in the pure gelatin sample. This indicates that the gelatin structure remains intact even after the ultrasonic irradiation. The observed peaks also have reduced intensities for all the bands with the amide I band at around 1660 cm^{-1} shifted to 1640 cm^{-1} and similar shifts for the other bands as tabulated in Table 2.

The vibrational modes of interest here are those due to the C=O, C-N, C-N-H and C-H species. These show absorption peaks in the regions of 1550 cm^{-1}, 1644 cm^{-1}, and 2925 cm^{-1} as indicated in Table 2. Figures 4 contain expanded spectra for these regions of interest for the

ACCEPTED MANUSCRIPT

400 °C reaction temperature samples and the pure gelatin sample. To compare the spectra accurately, the plots of the Gel-HAP samples have the same scale in the x- and y- coordinates. The results for the amide I & amide II bending mode, Carbonyl stretching mode and C-H stretch mode, as observed in the pure gelatin, confirm that gelatin has been incorporated into the nano HAP phase. It is interesting to note that the 2 ml Gel-HAP sample contained very small amounts of gelatin initially, show the amide, carbonyl species arising from the gelatin. Another point of interest is that at the reaction temperature of 400 °C, all samples with gelatin still show the amide and carbonyl species.

Figures 5a, 5b, 5c and 5d show the FE-SEM images of the samples treated at 400 °C. These images are similar to those obtained for the 100 °C, 200 °C and 300 °C samples. The images show small spherical particles agglomerated into clusters. The Gel-HAP particle size is similar to a previous study [34] but the topography is different to the pure nano HAP synthesized by use of ultrasound irradiation. The nano particles in Gel-HAP are more agglomerated into larger clusters and it appears that there are various different agglomerations of nano sized pores in between the fine particles. The average size of the particles, from the SEM images, is determined to be 29 nm ± 5%, agreeing with the calculated grain size from the XRD spectra.

Emulsification and homogenization are physical effects obtained through interaction of ultrasonic waves within a liquid medium and are responsible for morphological differences and ordered structures. Particles formed during the process of sonolysis can modify surface groups of the gelatin species as discussed by Jevtic *et al.* [39]. The presence of gelatine during the growth phase of the HAP in a low-power ultrasonic field promotes lesser adhesion and results in a smaller and less regular spheroid shape of the Gel-HAP nano particles.

ACCEPTED MANUSCRIPT

Low powered ultrasound irradiation has assisted in the synthesis of nano Gel-HAP material and in the interaction processes between gelatine and the nano HAP particles. The amide and carbonyl species from the gelatine subsequently attach to the HAP nano particles during the growth phase via ultrasonic assisted chemical interaction. This also enhanced the particles capability to conglomerate into groups or clusters in a more or less homogenous topography.

4.0 Conclusion

Whilst many studies have investigated large concentrations of gelatine-HAP composites using many traditional techniques, this study investigates a combination of low powered ultrasonic irradiation and low concentration of gelatin in the synthesis of nano Gel-HAP. The synthesized nano Gel-HAP has an average particle size of 29 nm ± 5% and a different morphology from pure Nano-HAP by the same ultrasonic method. XRD studies have shown that the synthesised Gel-HAP nano particles, contains a purer HAP phase. Features investigated with SEM and FT-IR indicates that the Gel-HAP nano particles are spherical in shape and conglomerate. Low power ultrasonic irradiation and temperature treatment plays a vital role in determining the size, morphology phase of the manufactured Gel-HAP samples. The presence of incorporated gelatine in the resulting nano structured hydroxyapatite after thermal treatment makes this material favourable for potential bone tissue engineering applications.

ACCEPTED MANUSCRIPT

ACCEPTED MANUSCRIPT

Acknowledgement

The authors thank Professor Li De-Yu (Curtin University of Technology) and Professor Phillip Jennings (Murdoch University) for their valuable discussions on the project. This work was supported by the Western Australian Nanochemistry Research Institute (WANRI) and Dr Zhong-Tao Jiang and Dr Derek Fawcett wishes to thank WANRI for a Research Fellowship. from WANRI.

References

[1] J.P. Fisher, Tissue Engineering, CRC Press, Hoboken, 2007, ISBN:9781420008333.

[2] P.Q. Ruhe, J.G.C. Wolke, P.H.M. Spauwen, J.A. Jansen, Calcium phosphate ceramics for bone tissue engineering, in: Tissue Engineering, ed. J. P. Fisher, A. G. Mikos, CRC Press LLC, 2007, pp. 9/1–9/18.

[3] E.E. Falco, J.S. Roth, J.P. Fisher, EH networks as a scaffold for skeletal muscle regeneration in abdominal wall hernia repair, J. Surg. Res. 149 (2008) 76-83.

[4] W. Mitchell, J.B. Matthews, M.H. Stone, J. Fisher, E. Ingham, Comparison of the response of human peripheral blood mononuclear cells to challenge with particles of three bone cements in vitro, Biomaterials 24 (2003) 737-748.

[5] J.P. Fisher, D. Dean, A.G. Mikos, Photocrosslinking characteristics and mechanical properties of diethyl fumarate/poly(propylene fumarate) biomaterials, Biomaterials 23 (2002) 4333-4343.

[6] B. Wopenka, J.D. Pasteris, A mineralogical perspective on the apatite in bone, Materials Science and Engineering C 25 (2005) 131-143.

[7] C. Hellmich, F.J. Ulm, Average hydroxyapatite concentration is uniform in the extracollagenous ultrastructures of mineralized tissues: evidence at the 1-10 microm scale, Biomechan. Model. Mechanobiol. 2 (2003) 21-36.

[8] C. F. Nawrot, D. J. Campbell, A Chromatographic Study of the Relative Affinities of Rat Bone and Skin Collagen 1 Chains for Hydroxyapatite, J. Dent. Res. 56 (1977) 1017-1022.

[9] W.F. Neuman, M.W. Neuman, The chemical dynamics of bone mineral, Chicago, The University of Chicago Press, 1958.

[10] S. Santavirta, Y.T. Konttinen, R. Lappalainen, A. Anttila, S.B. Goodman, M. Lindo, L.Smith, M. Takagi, E. Gomez-Barrena, L. Nordsletten, J.W. Xu, Materials in total

ACCEPTED MANUSCRIPT

joint replacement, Current Orthopaedics 12 (1998) 51-57.

[11] S.J. Kalita, A. Bhardwaj, H.A. Bhatt, Nanocrystalline calcium phosphate ceramics in biomedical engineering, Materials Science and Engineering C 27 (2007) 441-449.

[12] H.R.R. Ramay, M. Zhang, Biphasic calcium phosphate nanocomposite porous scaffolds for load-bearing bone tissue engineering, Biomaterials 25 (2004) 5171-5180.

[13] M.H. Fathi, A. Hanifi, V. Mortazavi, Preparation and bioactivity evaluation of bone-like hydroxyapatite nanopowder, Journal of Materials Processing Technology 202 (2008) 536-542.

[14] Z. Shi, X. Huang, Y. Cai, R. Tang, D. Yang, Size effect of hydroxyapatite nanoparticles on proliferation and apoptosis of osteoblast-like cells, Acta Biomater. 5 (2009) 338-345.

[15] J. Hu, Z.S. Liu, S.L Tang, Y.M. He, Effect of hydroxyapatite nanoparticles on the growth and p53/c-Myc protein expression of implanted hepatic VX2 tumor in rabbits by intravenous injection, World J. Gastroenterol. 13 (2007) 2798-2802.

[16] J. Li, Y. Yin, F. Yao, L. Zhang, K. Yao, Effect of nano- and micro-hydroxyapatite/chitosan-gelatin network film on human gastric cancer cells, Materials Letters 62 (2008) 3220-3223.

[17] N. Sasaki, H. Umeda, S. Okada, R. Kojima, A. Fukuda, Mechanical properties of hydroxyapatite-reinforced gelatin as a model system of bone, Biomaterials 10 (1989) 129-132.

[18] X. Cai, H. Tong, X. Shen, W. Chen, J. Yan, J. Hu, Preparation and characterization of homogeneous chitosan-polylactic acid/hydroxyapatite nanocomposite for bone tissue engineering and evaluation of its mechanical properties, Acta Biomater. 5 (2009) 2693-2703.

[19] S.K. Roy Chowdhury, A.C. Kulkarni, A. Basak, S.K. Roy, Wear characteristic and biocompatibility of some hydroxyapatite-collagen composite acetabular cups, Wear 262 (2007) 1387-1398.

[20] M.C. Chang, C.C. Ko, W.H. Douglas, Preparation of hydroxyapatite-gelatin nanocomposite, Biomaterials 24 (2003) 2853-2862.

[21] M. Ngiam, S. Liao, A.J. Patil, Z. Cheng, C.K. Chan, S. Ramakrishna, The fabrication of nano-hydroxyapatite on PLGA and PLGA/collagen nanofibrous composite scaffolds and their effects in osteoblastic behavior for bone tissue engineering, Bone 45 (2009) 4-16.

[22] Y.S. Pek, S. Gao, M.S.M. Arshad, K.J. Leck, J.Y. Ying, Porous collagen-apatite nanocomposite foams as bone regeneration scaffolds, Biomaterials 29 (2008) 4300-4305.

ACCEPTED MANUSCRIPT

ACCEPTED MANUSCRIPT

[23] H.W. Kim, H.E. Kim, V. Salih, Stimulation of osteoblast responses to biomimetic nanocomposites of gelatin-hydroxyapatite for tissue engineering scaffolds, Biomaterials 26 (2005) 5221-5230.

[24] C. Shu, Y. Xianzhu, X. Zhangyin, X. Guohua, L. Hong, Y. Kangde, Synthesis and sintering of nanocrystalline hydroxyapatite powders by gelatin-based precipitation method, Ceramics International 33 (2007) 193-196.

[25] T. Bera, A.N. Vivek, S.K. Saraf, P. Ramachandrarao, Characterization of biomimetically synthesized Hap–Gel nanocomposites as bone substitute, Biomed.Mater. 3 (2008) 025001.

[26] J. Sundaram, T.D. Durance, R. Wang, Porous scaffold of gelatin-starch with nanohydroxyapatite composite processed via novel microwave vacuum drying, Acta Biomater. 4 (2008) 932-942.

[27] W.B. Hillig, Y. Choi, S. Murtha, N. Natravali, P. Ajayan, An open-pored gelatin/hydroxyapatite composite as a potential bone substitute, J. Mater. Sci. Mater. Med. 19 (2008) 11-17.

[28] H.W. Kim, J.C. Knowles, H.E. Kim, Hydroxyapatite and gelatin composite foams processed via novel freeze-drying and cross linking for use as temporary hard tissue scaffolds, J. Biomed. Mater. Res. A 72A (2005) 136-145.

[29] C. Shu, Y. Xianzhu, X. Zhangyin, X. Guohua, L. Hong, Y. Kangde , Synthesis and sintering of nanocrystalline hydroxyapatite powders by gelatine-based precipitation method, Ceramics International 33 (2007) 193-196.

[30] X. Li, J. Xie, X. Yuan, Y. Xia, Coating Electrospun Poly(ε-caprolactone) Fibers with Gelatin and Calcium Phosphate and Their Use as Biomimetic Scaffolds for Bone Tissue Engineering, Langmuir 24 (2008) 14145-14150.

[31] S. Teng, L. Chen, Y. Guo, J. Shi, Formation of nano-hydroxyapatite in gelatin droplets and the resulting porous composite microspheres, J. Inorg. Biochem. 101 (2007) 686-691.

[32] Y.J. Yin, F. Zhao, X.F. Song, K.D. Yao, W.W. Lu, J.C. Leong, Preparation and characterization of Hydroxyapatite/Chitosan–Gelatin Network Composite, Journal of Applied Polymer Science, 77 (2000) 2929–2938.

[33] R.A. Hule, D. Pochan, Polymer Nanocomposites for Biomedical Applications, Mrs Bulletin 32 (2007) 354-358.

[34] M. Jevtic, M. Mitric, S. skapin, B. Jancar, N. Ignjatovic, D. Uskokovic, Crystal Structure of Hydroxyapatite Nanorods Synthesized by Sonochemical Homogeneous Precipitation, Crystal Growth & Design 8 (2008) 2217-2222.

[35] A. Ethirajan, U. Ziener, A. Chuvilin, U. Kaiser, H. Colfen, K. Landfester, Biomimetic Hydroxyapatite Crystallization in Gelatin Nanoparticles Synthesized Using a Miniemulsion Process, Advanced Functional Materials 18 (2008) 2221–2227.

ACCEPTED MANUSCRIPT

[36] G.E. Poinern, R.K. Brundavanam, N. Mondinos, Z.T. Jiang, Synthesis and characterisation of nanohydroxyapatite using an ultrasound assisted method, Ultrason. Sonochem. 16 (2009) 469-474.

[37] V.M. Rusu, C.H. Ng, M. Wilke, B. Tiersch, P. Fratzl, M.G. Peter, Size-controlled hydroxyapatite nanoparticles as self-organized organic–inorganic composite materials, Biomaterials 26 (2005) 5414-5426.

[38] S.N. Danilchenko, O.G. Kukharenko, C. Moseke, I.Y. Protesnko, L.F. Sukhodub, B. Sulkio-Cleff, Determination of the Bone Mineral Crystallite Size and Lattice Strain from Diffraction Line Broadening, Cryst. Res. Technol. 37 (2002) 1234-1240.

[39] J.C. Elliott, Chapter 3, Structure and Chemistry of the Apatites and Other Calcium Orthophosphastes, Elsevier, London (1994).

[40] M. Jevtic, A. Radulovic, N. Ignjatovic, M. Mitric , D. Uskokovic, Controlled assembly of poly (D,L-lactide-co-glycolide)/hydroxyapatite core–shell nanospheres under ultrasonic irradiation, Acta Biomater. 5 (2009) 208–218.

[41] J.H. Muyonga, C.G.B. Cole, K.G. Duodu, Characterisation of acid soluble collagen from skins of young and adult Nile perch (Lates niloticus), Food Chemistry 86 (2004) 325–332.

[42] N.P. Camacho, P. West, P.A. Torzilli, R. Mendelsohn, FTIR Microscopic imaging of colloagen and proteoglycan in Biovine Cartilage, Biopolymers 62 (2001) 1–8.

Figure Captions

1. Figure 1: XRD patterns of HAP and Gel-HAP (0, 2, 40, 100 ml Gel.Sol.) powders thermally treated at T = 400°C. The (h k l) indices show the main HAP phase. ○ Indicates Calcium Hydrogen Phosphate Hydroxide phases in the samples.
2. Figure 2: FT-IR spectra of HAP/Gel-HAP (0, 2, 40, 100 ml Gel.Sol.) powders thermally treated at T = 400°C.
3. Figure 3: FT-IR spectra of Gelatine.
4. Figure 4: FT-IR patterns (C-H Stretch) for (i) Nano HAP, (ii) Gel-HAP (2 ml Gel.Sol.) , (iii) Gel-HAP (40 ml Gel.Sol.), (iv) Gel-HAP (100 ml Gel.Sol.) and (v) Pure gelatin. All the samples were treated at T = 400°C.
5. Figure 5: 5a, 5b are FE-SEM images of a Gel-HAP sample after heat treatment at 400°C temperatures, (scale bar = 200 nm). 5c and 5d are higher resolution images of same sample, (scale bar = 100 nm).

ACCEPTED MANUSCRIPT

Table Captions

1. Table 1: Particle size (nm) calculated from XRD in terms of ultrasonic power, dilute gelatine concentrations and preparation temperature.
2. Table 2: FT-IR Absorption band measurements for HAP and Gel-HAP (2, 40, 100 ml Gel.Sol.) powdered samples (different ultrasonic power) treated at T= 400°C.

Supplementary Figure Captions:

1. Figure 1: Author preparing nano Gel-HAP using UP50H (50 W, 30 kHz).
2. Figure 2: Experimental procedure for nano Gel-HAP preparation.
3. Figure 3a: The XRD patterns for nano Gel-HAP powders with various dilute concentrations of gelatine solutions (0, 2, 40 and 100 ml) thermally treated at T = 100°C. The (h k l) indices show the main HAP phase.
4. Figure 3b: The XRD patterns for nano Gel-HAP powders with various dilute concentrations of gelatine solutions (0, 2, 40 and 100 ml) thermally treated at T = 200°C. The (h k l) indices show the main HAP phase.
5. Figure 3c: The XRD patterns for nano Gel-HAP powders with various dilute concentrations of gelatine solutions (0, 2, 40 and 100 ml) thermally treated at T = 300°C. The (h k l) indices show the main HAP phase.
6. Figure 3d: The XRD patterns for nano Gel-HAP powders with various dilute concentrations of gelatine solutions (0, 2, 40 and 100 ml) thermally treated at T = 400°C. The (h k l) indices show the main HAP phase.
7. Figure 4a: FT-IR patterns (amide I bending) for (i) Nano HAP, (ii) Gel-HAP (2 ml Gel.Sol.), (iii) Gel-HAP (40 ml Gel.Sol.), (iv) Gel-HAP (100 ml Gel.Sol.) and (v) Pure gelatin. All the samples were treated at T = 400°C.
8. Figure 4b: FT-IR patterns (amide II bending) (i) Nano HAP, (ii) Gel-HAP (2 ml Gel.Sol.), (iii) Gel-HAP (40 ml Gel.Sol.), (iv) Gel-HAP (100 ml Gel.Sol.) and (v) Pure gelatin. All the samples were treated at T = 400°C.

ACCEPTED MANUSCRIPT

ACCEPTED MANUSCRIPT

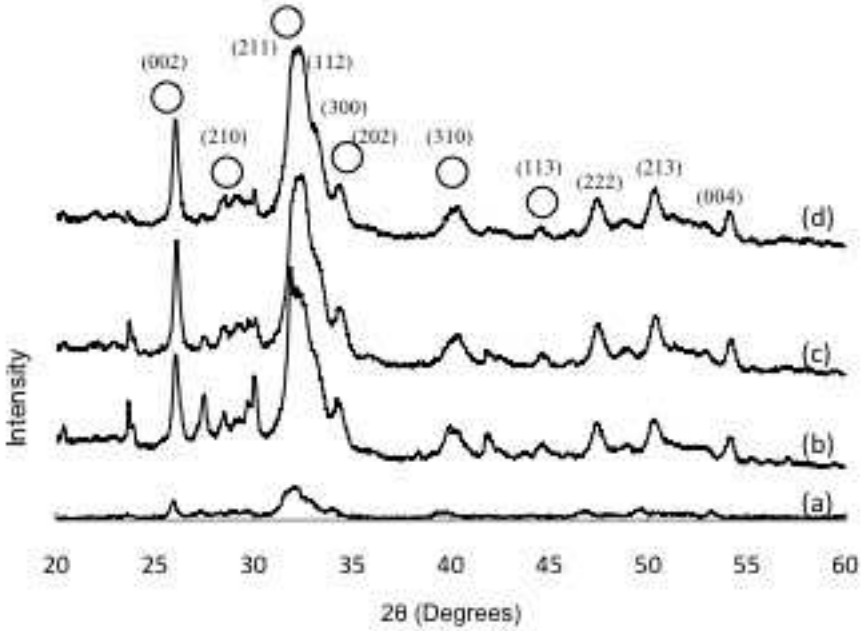

(a) Pure HAP, (b) Gel-HAP (2 ml Gel.Sol.),
(c) Gel-HAP (40 ml Gel.Sol.), (d) Gel-HAP (100 ml Gel.Sol.)

(i) **No Ultrasonic Irradiation**

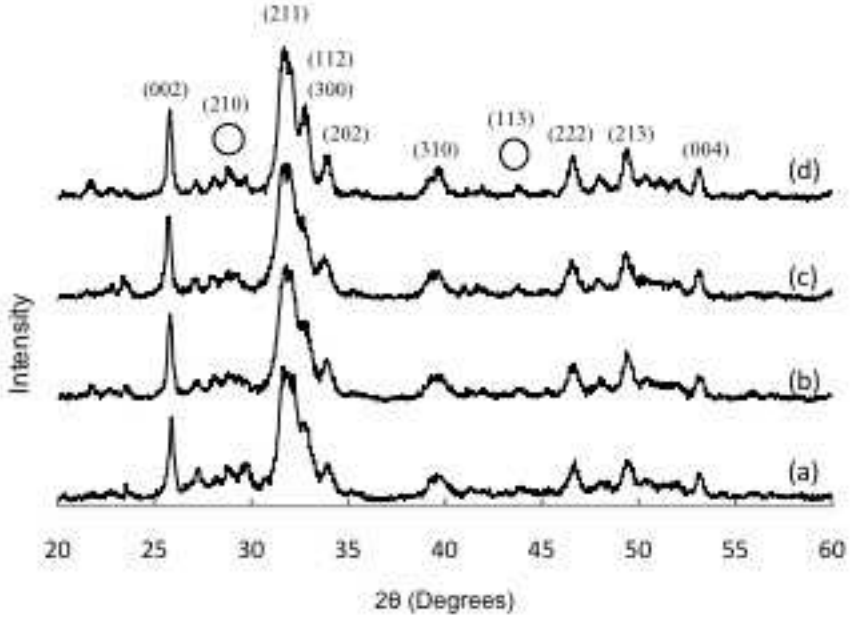

(a) Pure HAP, (b) Gel-HAP (2 ml Gel.Sol.),
(c) Gel-HAP (40 ml Gel.Sol.), (d) Gel-HAP (100 ml Gel.Sol.)

(ii) **Ultrasonic Irradiation**

Figure 1: XRD patterns of HAP and Gel-HAP (0, 2, 40, 100 ml Gelatine solution) powders thermally treated at T = 400°C . Samples in (i) are not treated with ultrasound and samples in (ii) are treated with ultrasound. ○ indicates Calcium Hydrogen Phosphate Hydroxide phases in the samples. The (h k l) indices show the main HAP phase.

ACCEPTED MANUSCRIPT

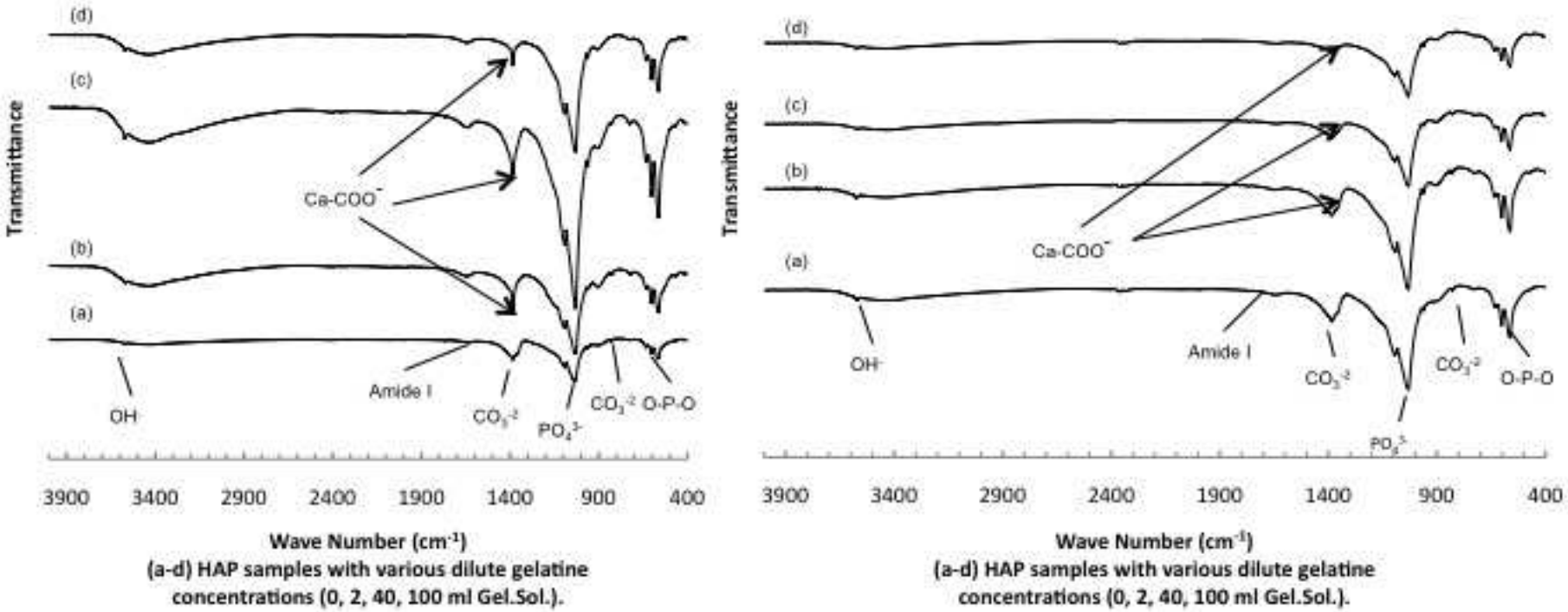

Figure 2: FT-IR spectra of HAP/Gel-HAP (0, 2, 40, 100 ml Gel.Sol.) powders thermally treated at T = 400°C.

ACCEPTED MANUSCRIPT

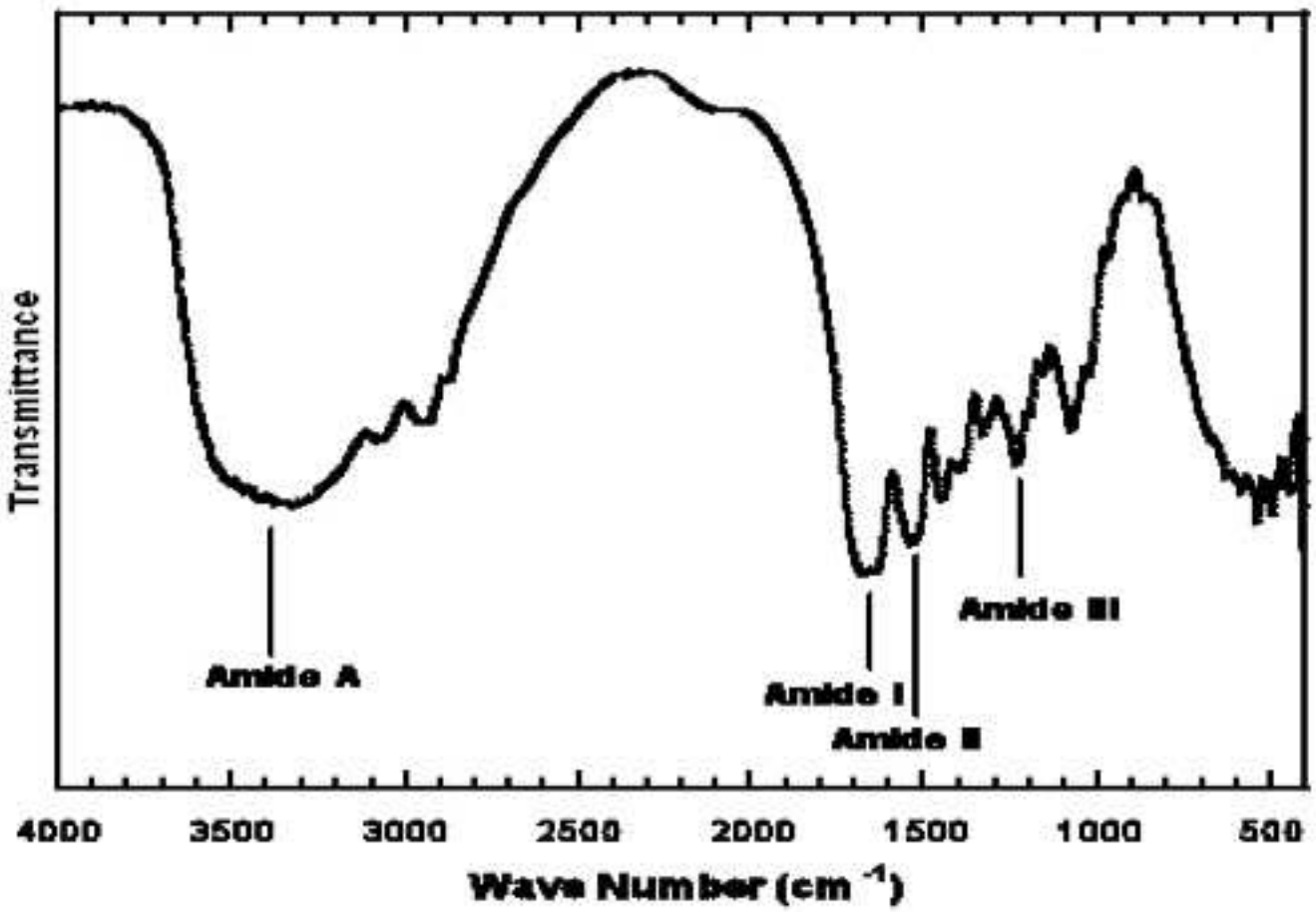

Figure 3: FT-IR spectra of Gelatine

ACCEPTED MANUSCRIPT

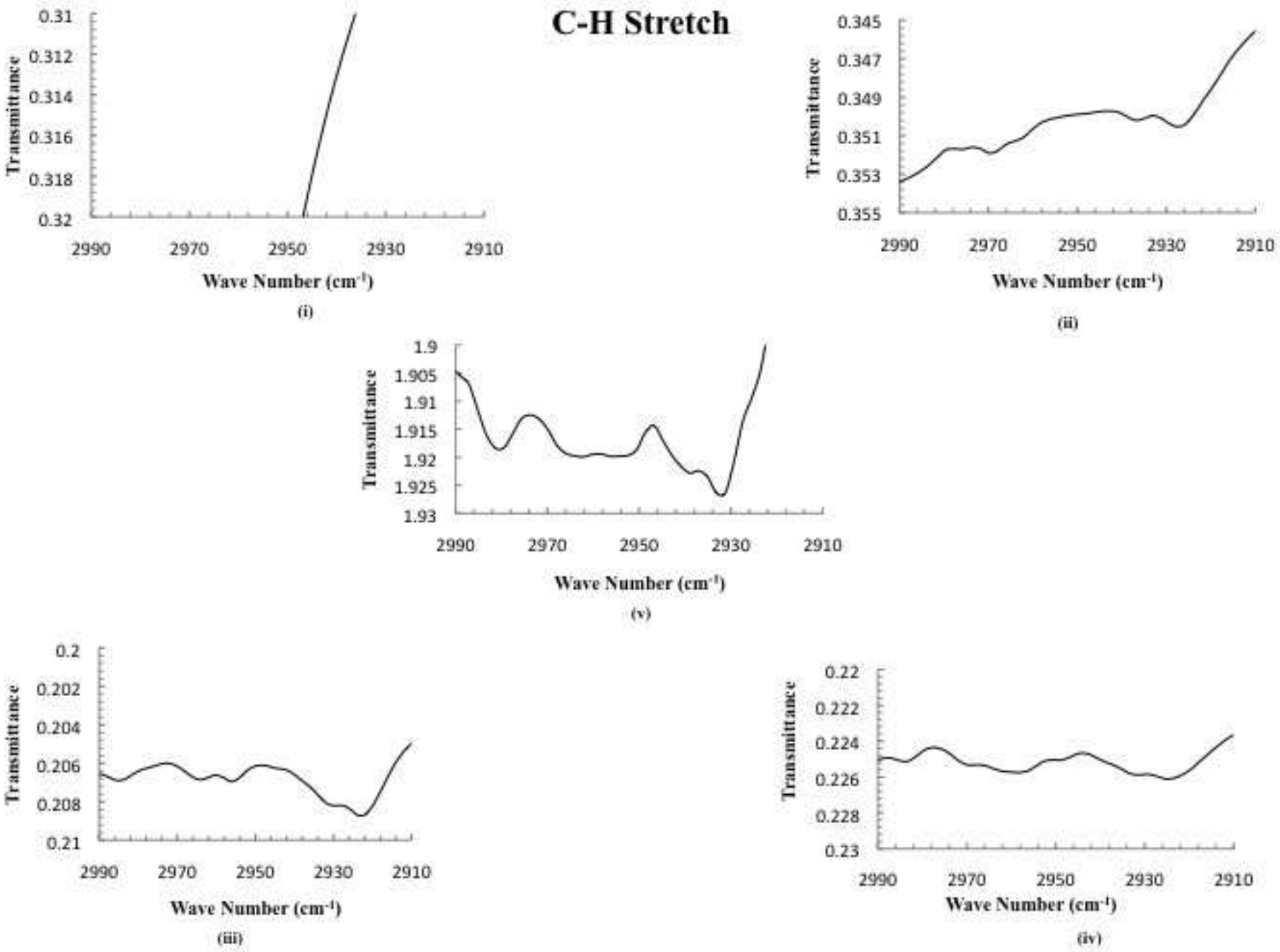

Figure 4: FT-IR patterns (C-H Stretch) for (i) Nano HAP, (ii) Gel-HAP (2 ml Gel.Sol.) , (iii) Gel-HAP (40 ml Gel.Sol.), (iv) Gel-HAP (100 ml Gel.Sol.) and (v) Pure gelatin. All the samples were treated at T = 400°C.

ACCEPTED MANUSCRIPT

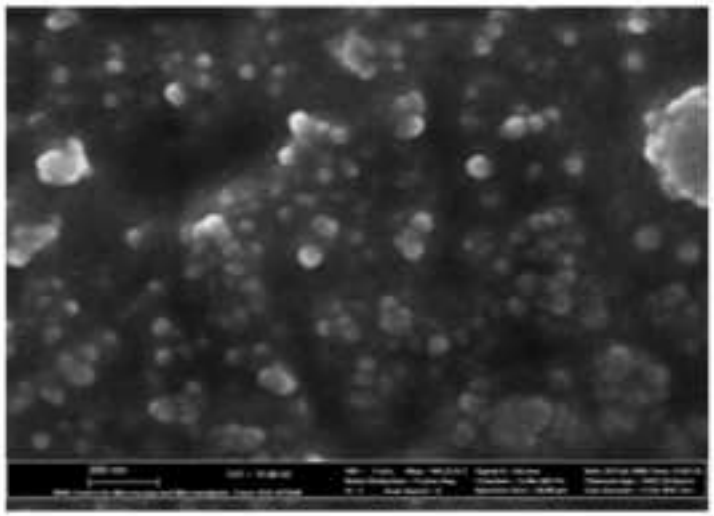

(5a)

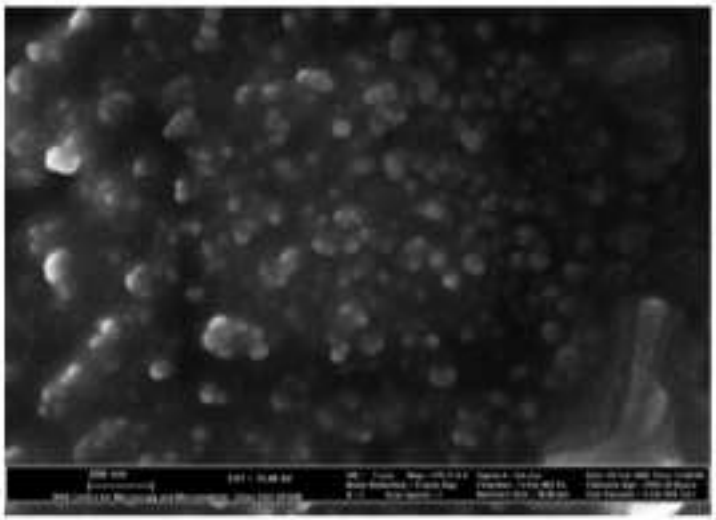

(5b)

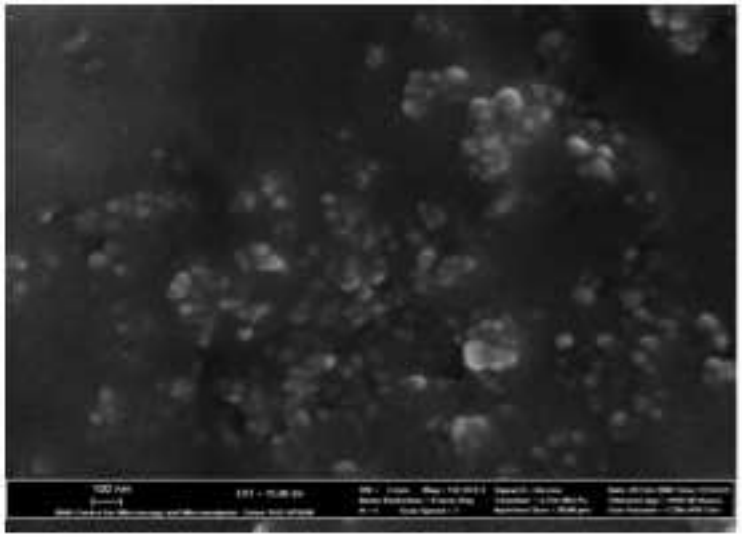

(5c)

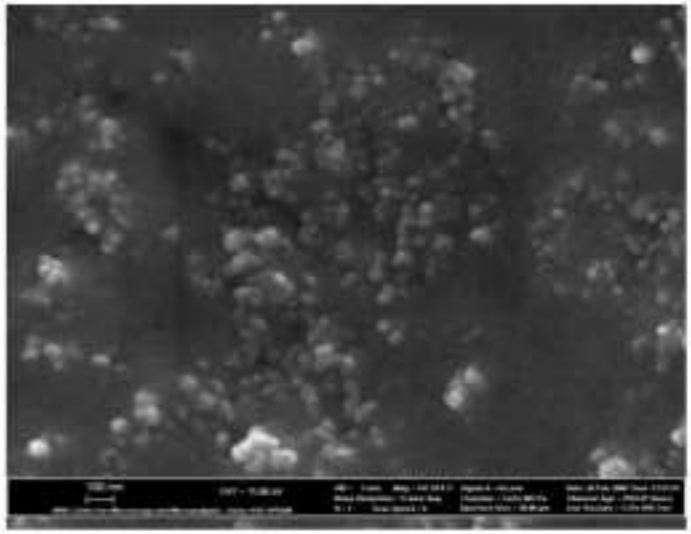

(5d)

Figure 5: 5a, 5b are FE-SEM images of a Gel-HAP sample after heat treatment at 400°C temperature, (scale bar = 200 nm). 5c and 5d are higher resolution images of same sample, (scale bar = 100 nm).

ACCEPTED MANUSCRIPT

Ultrasonic Power (W)	Particle Size (nm ± 5 %)				
	Gelatine concentration (ml)	100 °C	200 °C	300 °C	400 °C
0	0	230	230	230	180
	2	110	115	110	110
	40	92	95	95	92
	100	89	91	89	87
50	0	58	35	30	25
	2	33	28	33	33
	40	33	33	28	28
	100	39	33	33	28

Table 1: Particle size (nm) calculated from XRD in terms of ultrasonic power, dilute gelatine concentrations and preparation temperature.

ACCEPTED MANUSCRIPT

Ultrasonic Power (W)	Absorption Band	Wave Number (cm-1)				Vibrational mode
		HAP	2 ml	40 ml	100 ml	
0	PO_4^{3-}	1033, 1091 962,565,404	1031,1093 960,563,401	1031,1091 960,563,399	1031,1093 960,563,401	Asymmetric stretching Symmetric stretching
	OH^-	3571 632	3569 632	3569 632	3569 632	Stretching Asymmetric bending
	N-H	3432	3444	3440	3444	Symmetric Stretch
	H_2O	3415	3411	3428	3415	Stretching
	$Ca\text{-}COO^-$	1384	1384	1384	1384	Stretching
	CO_3^{-2}	831	827-833	827-833	827-833	v2 Out of plane bend
		1450-1470	1450-1470	1450-1470	1450-1470	v3 Symmetric stretch
	C=O	-	1643	1641	1641	Amide I bending (Carbonyl group stretch)
	C-N/C-N-H	-	1556, 1545	1559,1544	1552,1535	Amide II bending
	C-H	-	2929	2927	2923	Stretching
50	PO_4^{3-}	1038, 1091 968,571,410	1031,1093 962,565,401	1031,1093 962,565,404	1031,1093 962,565,404	Asymmetric stretching Symmetric stretching
	OH^-	3577 632	3571 632	3571 632	3577 634	Stretching Asymmetric bending
	N-H	3442	3446	3442	3438	Symmetric Stretch
	H_2O	3411	3415	3415	3415	Stretching
	$Ca\text{-}COO^-$	1377	1384	1384	1384	Stretching
	CO_3^{-2}	831	827-833	827-833	827-833	v2 Out of plane bend
		1450-1470	1450-1470	1450-1470	1450-1470	v3 Symmetric stretch
	C=O	-	1644	1643	1643	Amide I bending (Carbonyl group stretch)
	C-N/C-N-H	-	1556, 1538	1551,1544	1552,1536	Amide II bending
	C-H	-	2927	2923	2925	Stretching

Table 2: FT-IR Absorption band measurements for HAP and Gel-HAP (2, 40, 100 ml Gel.Sol.) powdered samples (different ultrasonic power) treated at T= 400°C.

ACCEPTED MANUSCRIPT

Research Highlights:

1. This study investigates the combination of low powered ultrasonic irradiation and low gelatine concentration in the synthesis of nano gelatine-hydroxyapatite (Gel-HAP) composites.

2. The synthesized nano Gel-HAP has an average particle size of 29 nm ± 5% and a different morphology from pure Nano-HAP using the same ultrasonic technique.

3. Low power ultrasonic irradiation and subsequent thermal treatment plays a vital role in determining the size, morphology, phase and symmetry of the manufactured nano Gel-HAP samples.

ACCEPTED MANUSCRIPT